Real-Time Sensing and Discrimination of Single Chemicals Using the Channel of Phi29 DNA Packaging Nanomotor

Farzin Haque,[†] Jennifer Lunn,[‡] Huaming Fang,[†] David Smithrud,[‡] and Peixuan Guo[†,*]

[†]Nanobiotechnology Center, Department of Pharmaceutical Sciences, and Markey Cancer Center, University of Kentucky, Lexington, Kentucky 40536, United States, and [‡]Department of Chemistry, University of Cincinnati, Cincinnati, Ohio 45267, United States

ABSTRACT A highly sensitive and reliable method to sense and identify a single chemical at extremely low concentrations and high contamination is important for environmental surveillance, homeland security, athlete drug monitoring, toxin/drug screening, and earlier disease diagnosis. This article reports a method for precise detection of single chemicals. The hub of the bacteriophage phi29 DNA packaging motor is a connector consisting of 12 protein subunits encircled into a 3.6 nm channel as a path for dsDNA to enter during packaging and to exit during infection. The connector has previously been inserted into a lipid bilayer to serve as a membrane-embedded channel. Herein we report the modification of the phi29 channel to develop a class of sensors to detect single chemicals. The lysine-234 of each protein subunit was mutated to cysteine, generating 12-SH ring lining the channel wall. Chemicals passing through this robust channel and interactions with the SH group generated extremely reliable, precise, and sensitive current signatures as revealed by single channel conductance assays. Ethane (57 Da), thymine (167 Da), and benzene (105 Da) with reactive thioester moieties were clearly discriminated upon interaction with the available set of cysteine residues. The covalent attachment of each analyte induced discrete stepwise blockage in current signature with a corresponding decrease in conductance due to the physical blocking of the channel. Transient binding of the chemicals also produced characteristic fingerprints that were deduced from the unique blockage amplitude and pattern of the signals. This study shows that the phi29 connector can be used to sense chemicals with reactive thioesters or maleimide using single channel conduction assays based on their distinct fingerprints. The results demonstrated that this channel system could be further developed into very sensitive sensing devices.

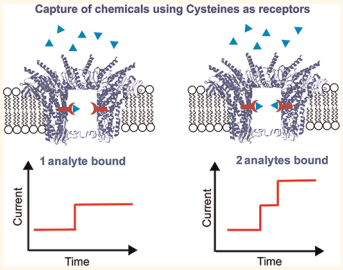

KEYWORDS: nanotechnology · nanobiotechnology · nanomotor · DNA packaging motor · bacteriophage phi29 · nanopore · sensing

Biological systems contain a wide variety of nanomachines and highly ordered macromolecular structures with diverse biological functions. Double-stranded (ds) DNA viruses package their genome into a preformed protein shell with the aid of a motor.[1−3] Bacterial virus phi29 DNA-packaging nanomotor with its elegant and elaborate channel has inspired its application in nanotechnology. This motor[4,5] uses ATP as energy and is composed of (1) a central protein core called the connector,[6,7] (2) six copies of pRNA (packaging RNA),[8−11] and (3) an ATPase gp16. The connector is composed of 12 copies of protein gp10, which encircle to form a dodecameric channel that acts as a pathway for the translocation of dsDNA. This ATP-driven DNA-packaging feature is common in other viruses, as well, such as T4,[12−16] λ,[17−20] HK97,[21] T3,[22] T7,[23,24] HSV,[25−29] adenovirus,[30−32] and poxvirus.[33,34] Although the individual building blocks of the connector of different viruses share little sequence homology and exhibit large variations in molecular weight,[7,26,35−39] the connector complexes possess a significant amount of morphological similarity.[40] In the case of bacteriophage phi29, the structure of the connector has been determined to atomic resolution.[7,35] The connector ring consists of 12 subunits, with a central channel formed by three long α-helices of each subunit. The ring is 13.8 nm at its wide end and 6.6 nm at its narrow end (Figure 1). The cross-sectional area of the channel is 10 nm^2 (3.6 nm in diameter) at the narrow end and 28 nm^2 (6 nm in diameter) at its wider end (Figure 1).[6,7,35] The wider end of the connector is located within the capsid, while the narrow end partially protrudes out of the capsid.

We recently inserted the connector into a lipid bilayer, and the resulting system has been shown to exhibit robust properties and generate extremely reliable, precise, and sensitive conductance signatures when ions or DNA pass through the channel, as revealed by single channel conductance measurements.[41,42] The connector channel exhibits one-way traffic property for DNA translocation from N-terminal entrance to C-terminal exit with a valve mechanism of DNA packaging.[43] Explicit engineering of the phi29 connector[44−50] is possible due

* Address correspondence to guop@purdue.edu.

Received for review January 12, 2012 and accepted March 29, 2012.

Published online March 29, 2012
10.1021/nn3001615

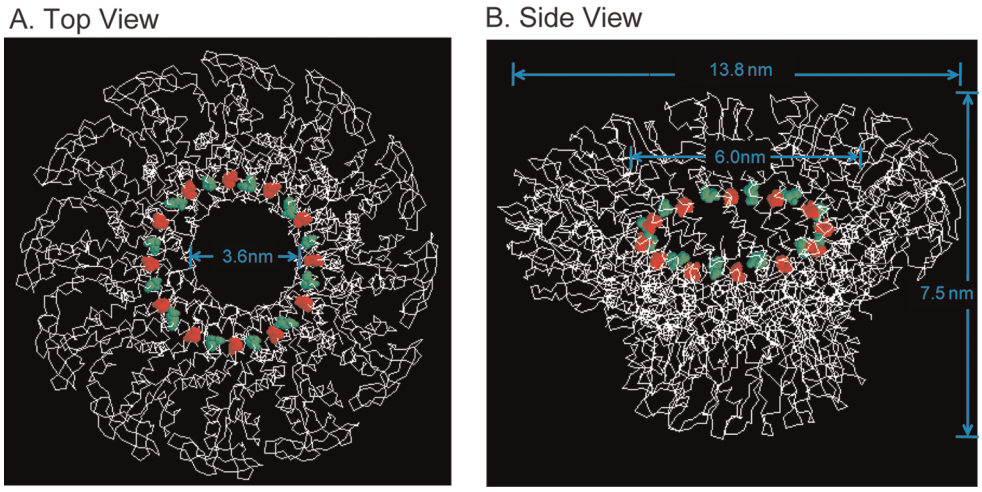

Figure 1. Structure of phi29 DNA-packaging motor connector showing the location of the cysteine ring and the dimensions of the channel. Top view (A) and side view (B) of phi29 connector showing the location of the tunnel loop N229 (green) and N246 (red). K234C is located within the tunnel loops shown.

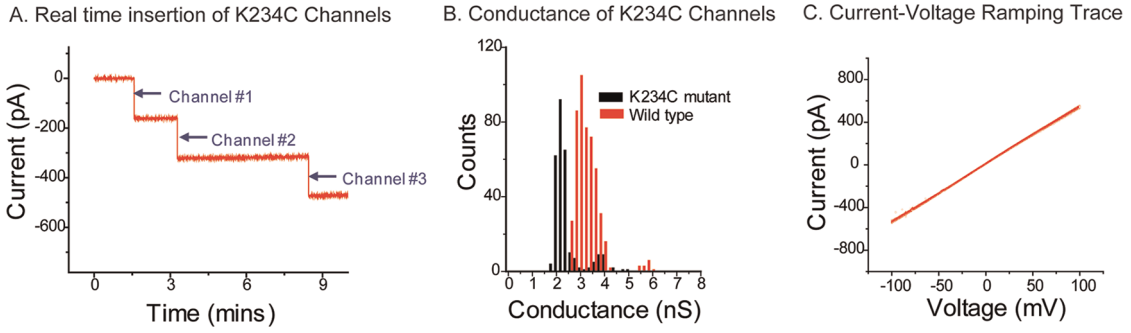

Figure 2. (A) Current trace showing continuous insertions of single K234C connectors into BLM. (B) Histogram of conductance measurements for single insertion under a specific voltage −75 mV (red, wild-type connector, *N* = 500; black, K234C connectors, *N* = 275). (C) Current−voltage trace under a ramp voltage from −100 to 100 mV (2.2 mV/s). All experiments were performed in the presence of 5 mM Tris (pH 7.8) with 1 M NaCl under −75 mV.

to its available crystal structure.[6,7,35] The pore size is nearly identical from sample to sample, and chemical conjugations within the large cavity of the pore can therefore be made with relative ease for added functionality. Procedures for large-scale production and purification of the connector have already been developed.[41,44,45,48,51,52] These features make the channel an ideal building block to produce a variety of semisynthetic receptors with predictable and reliable properties.[48−50]

Nanopore-based sensory techniques have been extensively used for the detection of a myriad of biomedical targets, from metal ions, drug compounds, and cellular second messengers to proteins and DNA.[53−70] Engineered transmembrane channels have the potential for stochastic detection, an approach relying on the real-time observation of individual binding events between single substrate molecules and a receptor.[71−73] Protein pores can be selectively functionalized with various probes that can bind individual target molecules with high selectivity and sensitivity.[74−76] The characteristic binding and distinctive current signatures can reveal the identity and concentration of the target analyte.[71,76] In addition, the dynamic interactions between the analyte and the binding sites can be studied in real-time at high resolution using single channel conduction assays.[75,77]

The ability to reengineer a biological nanomotor with atomic precision and incorporate it into lipid membranes will provide additional functionality as well as durability. Herein we report on the chemical modification of the phi29 channel as the first step in developing a class of sensors to detect single molecules. We introduced a cysteine ring within the channel wall and conjugated receptor modules within the channel wall.

RESULTS

Introduction of Cysteine Residues within the Channel Wall. The phi29 connector is composed of 12 copies of the protein gp10 with the central channel formed by three long helices of each subunit.[6,7,35,47,79−81] The connector has been inserted into a lipid bilayer, and the resulting system has been shown to exhibit robust properties and generate extremely reliable, precise, and sensitive conductance signatures when ions or DNA pass through the channel, as revealed by single channel conductance measurements.[41,42] The pore size is nearly identical (Figure 2A) from sample to

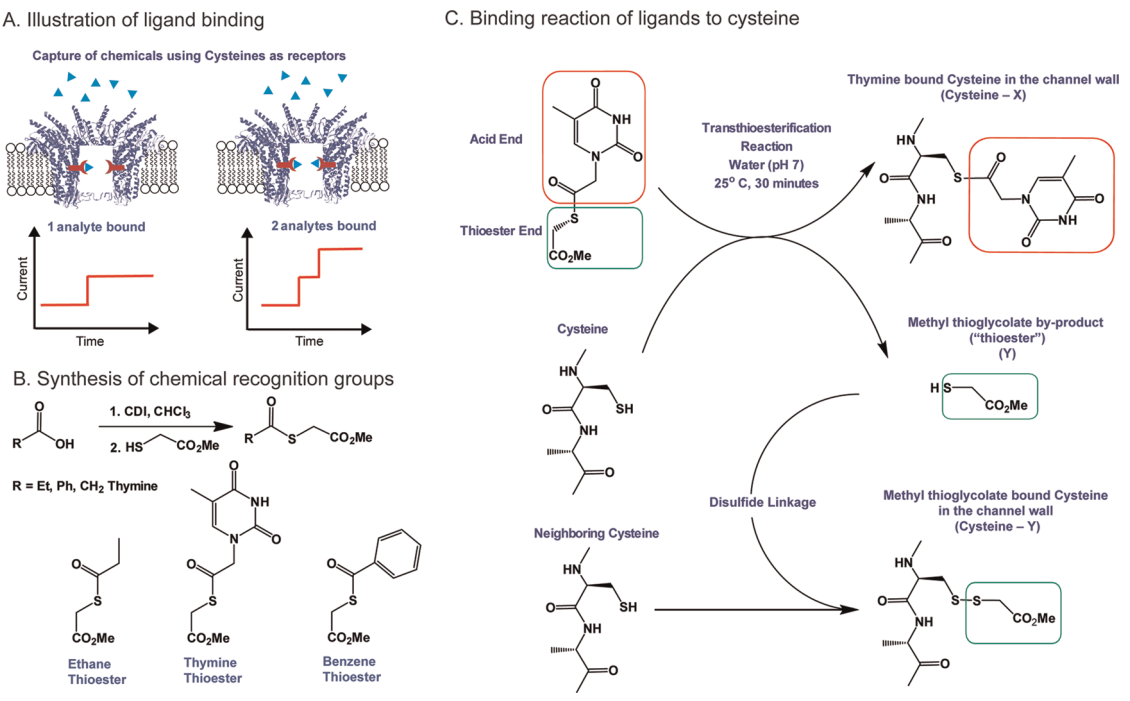

Figure 3. Conjugation of chemical ligands to channel wall resulted in the reduction of channel size as indicated by uniform stepwise blockage of channel current. (A) Schematic of ligand binding to the inner wall of the connector pore. (B) Synthesis of thioesters with ethane, thymine, and benzene moieties. (C) Transthioesterification method, showing that cysteines are readily modified with nucleobases when exposed to thioesters, using thymine thioester as an example; a second reaction *via* disulfide linkage results in the binding of the methyl thioglycolate byproduct.

sample, and chemical conjugations within the large cavity of the pore can therefore be made with relative ease for added functionality. The native connector contains two cysteine residues (C76 and C275) per gp10 protein that are buried within the wall and therefore are not accessible for conjugation of analytes or recognition moieties. Hence, accessible cysteines were introduced by mutagenesis within the inner wall of the connector, namely, the K234C mutant, where the lysine (K) was replaced with a cysteine (C) at the amino acid 234 position, located within the tunnel loop (Figure 1A,B). After assembly, the internal mutation generates a cysteine ring, composed of 12 evenly spaced residues in the same plane within the dodecameric connector channel (Figure 1).

Characterization of Cysteine Mutant Connector Channels in the Lipid Membrane. The K234C mutant connectors were first reconstituted into liposomes, followed by insertion into planar lipid membranes *via* vesicle fusion of liposome/connector complexes,[41] thereby forming a membrane-embedded nanopore system. The insertion of the K234C connector channels resulted in stepwise increase of the conductance, as shown in the continuous current trace (Figure 2A). The internal mutation did not affect the membrane insertion efficiency, signal stability, current homogeneity, membrane durability, and voltage gating properties.[41,42] However, the C-his K234C channels had a smaller cross-sectional area (conductance = 2.2 ± 0.17 nS) compared to the C-his connectors without the mutation (conductance = 3.2 ± 0.2 nS) (Figure 2B).[41,42] The conductance was calculated using the ratio of the measured current jump induced by a discrete step to the applied voltage. The step size of the connector channels was homogeneous (Figure 2B), and the channels exhibited equal conductance under both positive and negative transmembrane potentials. The channel conductance is uniform and demonstrates a perfectly linear *I*–*V* relationship without displaying any voltage gating phenomenon under the reported conditions of ±100 mV (Figure 2C).

Sensing and Discrimination of Ethane, Thymine, and Benzene Thioester Moieties. Common methods to selectively conjugate to the sulfhydryl side chain of cysteine residues include maleimides and iodoacetamides that form C–S bonds and sulfhydryls that form disulfides under oxidizing conditions. To determine the extent to which functional moieties can recognize, we adopted the well-known methodologies utilizing disulfide linkage or transthioesterification reactions[78] for conjugating various recognition groups to the cysteine residues exposed at the surface of the inner channel wall (Figure 3C).

The thioexchange reaction is highly chemoselective, rapid, and occurs in buffered aqueous solutions (pH 7), which appeared to be ideal for derivatizing the phi29 channel under conduction assay conditions. Binding events are characterized by monitoring the changes in the intensity of the current signal in a BLM setup (Figure 3A). The binding of chemicals sequentially to each cysteine probe induces stepwise blocks (a single molecule per block) in current with a corresponding decrease in conductance due to the physical

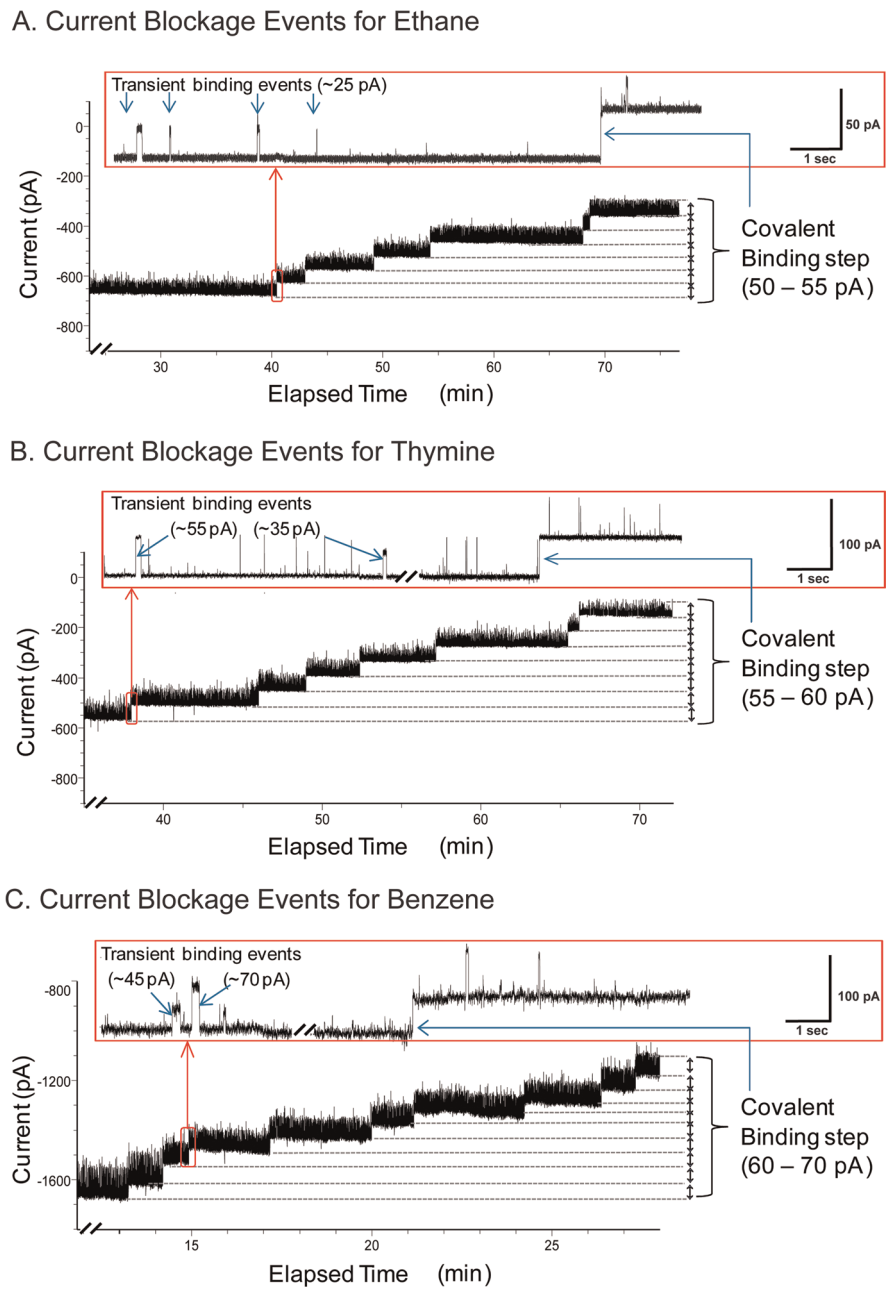

Figure 4. Data showing discrete blocking steps due to the binding of thioesters groups containing (A) ethane, (B) thymine, and (C) benzene. Inset: Magnified current trace showing the transient and permanent current blockage events.

blocking of the channel (Figure 4). The characteristic signature of the captured analyte is given by the unique blockage amplitude and pattern of the signals. The number of molecules bound can be counted from the stepwise blocks, and the concentration can be deduced from the number of binding events to a single pore per unit time.

The derivatized thioesters served as models to demonstrate the utility of the connector pore in capture and sensing (Figure 3A). The phenyl and thyminyl groups are similar in size, but the phenyl ring is hydrophobic and the thyminyl ring forms hydrogen bonds with water. The much smaller ethyl group truly tests the ability of the channel to sense small molecules. Two classes of current blockage signals were observed. The first class is the permanent binding event, which occurs through covalent bond formation between a thioester and a cysteine side chain of the channel *via* the transesterification reaction (Figure 3C). Permanent binding is displayed as discrete stepwise augment of current blockage (Figures 4 and 5C). The second class is the transient binding events induced by temporary binding of chemicals with the cysteines, as they pass through the channel and appear as the recoverable blockage signals (Figure 4, inset, and Figure 5A,B).

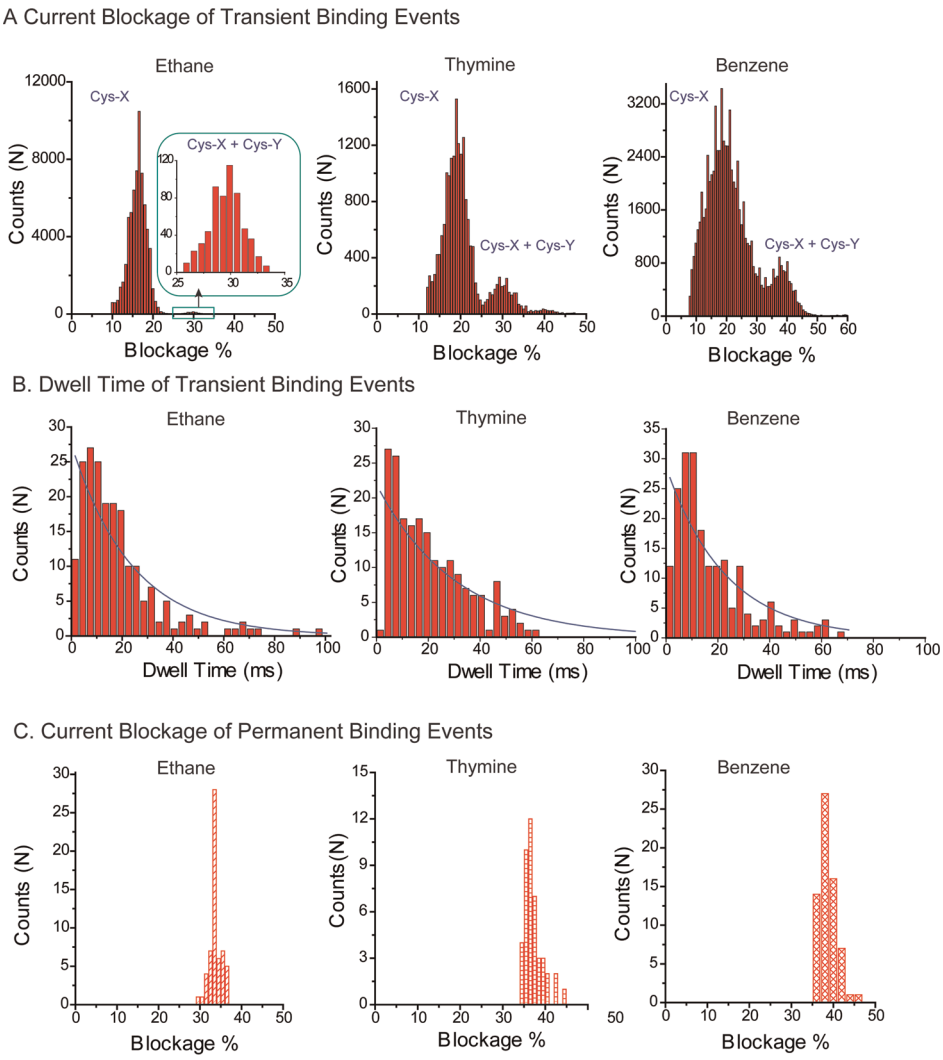

Figure 5. Analysis of current blockage events induced by thioesters. Histogram of transient current blockage events (A) with corresponding dwell time distributions (B) and permanent binding events (C) for the binding of thioesters groups containing ethane, thymine, and benzene, respectively. The dwell time data were fitted with a single exponential decay function (blue).

We found that the permanent binding events distinguished the ethane (C_3H_5O: 57 Da), thymine ($C_7H_7N_2O_3$: 167 Da), and benzene (C_7H_5O: 105 Da) thioester moieties that remain covalently attached to the channel wall (Figure 5C and Table 1B), with a characteristic channel current blockage of 33.5 $\pm$ 0.5, 36.3 $\pm$ 1.2, and 38.2 $\pm$ 2%, respectively (p value <0.001). These percentages represent the ratio of the open-pore current and the current reduction step induced by the individual binding events. The high permanent percent blockage value for the ethane moiety shows that this large channel is very sensitive to the presence of small molecules. The higher permanent percent blockage observed for the smaller sized benzene as compared to thymine shows that the shape or polarity of the molecule, besides the molecular weight, also contributed to the current blockage signature.

Although the transient signal represents the hit-and-run behavior (temporary binding interactions) of the chemicals, they can also be used to identify the ethyl, benzyl, or thyminyl groups (Figure 5A). Two transient signals, denoted components (Cys-X) and (Cys-X + Cys-Y), are observed for each thioester. Each set of signals is unique for a particular thioester (Figure 5A, Table 1A), and all transient percent blockage values are smaller than those observed for the corresponding permanent percent blockage value (Figure 5C, Table 1A,B). This result is surprising considering that the thioexchange reaction used to attach the compounds to the channel reduces the size of the molecule upon the cleavage and release of the thioester end (Figure 3C). One possible explanation is that the released thioester end (Y) binds concomitantly to the channel through disulfide bond formation (Cys-Y) during the same observable time frame as the thioexchange reaction, giving two molecules bound per channel (Cys-X + Cys-Y) for each step change in conductance (Figure 5A). We were unable, however, to attach the thioester directly through disulfide bond formation under the same reaction conditions.

TABLE 1. Analysis of Current Blockage Events

A. Thioesters: Transient Binding Events

	transient binding events		difference (%)		
thioesters	component (Cys-X)	component (Cys-X + Cys-Y)	components [(Cys-X + Cys-Y) − (Cys-X)] = (Cys-Y)	*p* value[a]	dwell time[b] (ms)
ethane	16.4 ± 2.0%	29.6 ± 1.4%	13.2 ± 2.4%	<0.822 (thymine); <0.189 (benzene)	23.8 ± 3.4
thymine	18.9 ± 2.6%	31.7 ± 2.2%	12.8 ± 3.4%	<0.822 (ethane); <0.184 (benzene)	30.5 ± 5.2
benzene	19.5 ± 6.2%	37.3 ± 3.7%	17.8 ± 7.2%	<0.189 (ethane); <0.184 (thymine)	23.0 ± 4.5

B. Thioesters: Permanent Binding Events

	transient binding events	permanent binding events		ratio of permanent to transient events	
thioesters	(Cys-X)	(Cys-X + Cys-X)	*p* value[c]	(Cys-X + Cys-X)(Cys-X)	*p* value[c]
ethane	16.4 ± 2.0%	33.5 ± 0.5% (*N* = 63)	<0.001(thymine); <0.001 (benzene)	2.04 ± 0.12	<0.001 (thymine); <0.065 (benzene)
thymine	18.9 ± 2.6%	36.3 ± 1.2% (*N* = 44)	<0.001 (ethane); <0.001 (benzene)	1.92 ± 0.14	<0.001 (ethane); <0.437 (benzene)
benzene	19.5 ± 6.2%	38.4 ± 2.0% (*N* = 66)	<0.001 (ethane); <0.001 (thymine)	1.96 ± 0.32	<0.065 (ethane); <0.437 (thymine)

C. Maleimide Binding Events

	transient binding events	permanent binding events	ratio of permanent to transient events	dwell time[d] (ms)
maleimide	17.0 ± 2.0%	38.1 ± 2.1% (*N* = 7)	2.2 ± 0.12	24.0 ± 4.8

[a] The *p* value is obtained from six independent experiments. [b] Derived from single exponential decay fit. [c] The *p* value is obtained using the number of covalent binding events for each thioester. [d] Derived from single exponential decay fit.

We further observed that the dwell time for all of the transient events for the three thioesters was ~25 ms (Table 1A). This relatively long dwell time implies that the transient events are indeed due to temporary binding of chemicals to the cysteine residues, rather than simple translocation through the pore. We cannot distinguish differences in dwell time between the two transient components (Cys-X) and (Cys-X + Cys-Y), implying that the disulfide bond formation (Cys-Y) occurs during the same observable time frame as the thioexchange reaction (Cys-X).

Two consistent findings were observed. The ratio of the permanent percent blockage signal and transient component (Cys-X) is ~2, implying that there are two thioesters bound per binding steps. Another interesting finding is that the difference between the percent blockage of the transient signals [component (Cys-X) − component (Cys-X + Cys-Y)] of ~13% for each set of transient signals reflects the temporary binding of the acid end of a thioester, which underwent hydrolysis in the solution phase. Accordingly, the ~13% would probably represent the loss of the thioester end, which is the consistent piece for all thioesters. We are currently designing experiments to assign the transient signals. These consistencies demonstrate that the channel is operating the same for each thioester, and the unique properties of a thioester control the set of percent blockage values. This means that, for these thioesters, three signals or fingerprints can be used singularly or in some combination to identify their presence within the channel.

Sensing of Maleimde Revealed a Consistent Blockage Ratio of 2 between Permanent and Transient Binding Events. Maleimide is a common reagent to link desired functional groups to cysteines. Accordingly, upon addition of maleimide to the conducting buffer, our single channel current measurements revealed only one type of transient binding event with a percent blockage of ~17% (Figure 6B,C). The permanent binding events with percent blockage of ~38% are ~2 times the transient events, which implies that two maleimide binding events occur per step (Figure 6, Table 1C). Similar dwell time of ~24 ms was observed for the transient binding events of maleimide (Table 1C).

The consistent observation was the ratio between permanent and transient signal (Table 1B), which ends up to be ~2 for all three thioesters investigated as well as for maleimide. Since the percent blockage values are different for each thioester and maleimide, it is unlikely due to the conformational change of the connector channel upon binding of the chemicals. Instead, a strong possibility is the simultaneous binding of two identical chemicals to neighboring cysteine residues, which probably stabilizes the housing of chemicals within the channel. Each channel can therefore accommodate an even number (2, 4, and maximum 6) of thioesters and maleimide moieties based on the percent blockage values.

DISCUSSION

Development of a highly sensitive detection system is important in many areas, including, but not limited to, pathogen identification, disease diagnosis, drug

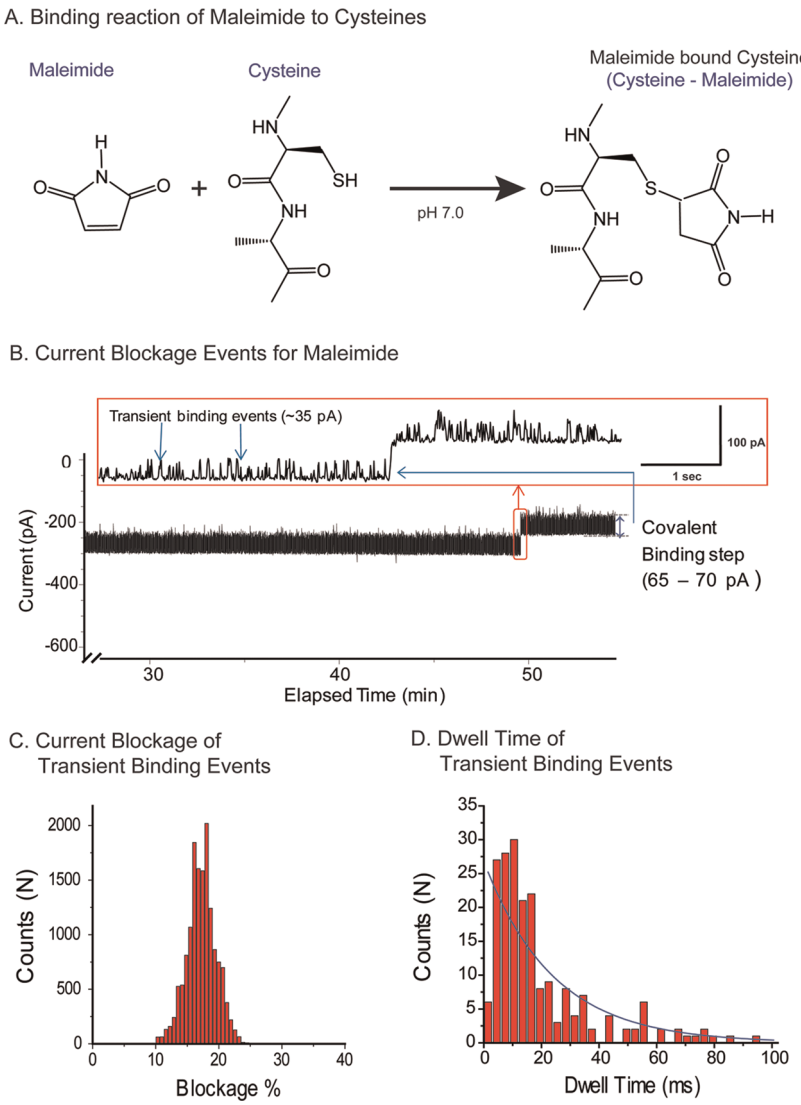

Figure 6. Conjugation of maleimide to channel wall. (A) Reaction scheme of maleimide–cysteine reaction. (B) Data showing discrete blocking steps due to the binding of maleimide. Inset: Magnified current trace showing the transient and permanent current blockage events. Histogram of transient current blockage events for maleimide (C) with corresponding dwell time distributions (D). The dwell time data were fitted with a single exponential decay function (blue).

screening, environmental monitoring, and national security. The detection of pathogens or toxins is analogous to the detection of criminals. The first step is the capture of a suspect by the police. The next step is the gathering of evidence, such as fingerprints, to serve as identification for court prosecution. The concept of "capture" has been used extensively in many sensing, detection, and diagnostic technologies that are currently available, such as antigen/antibody reactions,[82–84] biotin/streptavidin interactions,[85–89] ELISA,[90,91] and microarray-based technologies,[92–94] has been extensively used in practical applications. All of these techniques are well-developed and very useful; however, they possess a disadvantage in cases where the target substrate is at a very low concentration or when impurities are present at high concentrations. As a result, due to dissociation by a kinetic process, it is not possible to detect a single substrate molecule on a slide, regardless of how strong the signal of a single antibody is. This is because, at a very low concentration, the background noise will over-ride the specific signal from the antigen/antibody complex, and the antibody/complex will dissociate upon washing. The sensitivity issue is especially important in the early diagnosis of diseases and in environmental surveillance. When a small amount of chemical is spread on to the earth, the massive amount of materials in the environment will make it difficult to detect. The concept of "fingerprinting" has also been used extensively in the detection and diagnosis process. Examples include the spectrum pattern from spectroscopy, fluorescence, CD, NMR, and electrophysiological measurements of a single pore.[41–43,88,95–106] The same issue exists in that the impurity will result in a nonspecific signal and hinder the sensitivity and specificity due to the high background noise.

The results herein demonstrate that the phi29 channel is a sensor of very small compounds (the area of the

ethylthioester is approximately 60 Å^2) even though its interior volume is very large (approximately 1000 Å^2). Compounds are also differentiated based on their physical properties as well as their size. Sensing through the covalent derivatization of the channel produced an even larger percent blockage signal. This study showed that the phi29 can be used to sense chemically active thioesters in single channel conduction assays by observing a total of three readily observable fingerprints. Future experiments include using the permanently attached compounds within the channel to further fine-tune the phi29 channel sensor. Because the phi29 channel contains a large interior volume, attachment of a large variety of recognition domains is possible. Some domains could require the addition of two or more functional groups. We are currently developing methods to control the number of functional groups added to a channel and the pattern that they form. The proof-of-principle studies described here will be extended in the future to include multiple probes that can be constructed by engineering within a single pore for concurrent detection of multiple targets.

EXPERIMENTAL METHODS

Materials. Organic solvents (*n*-decane, hexane, choloroform, methylene chloride, and DMSO) were purchased from Sigma-Aldrich or Fisher. Moisture-sensitive reactions were carried out under positive argon pressure. ^{1}H NMR and ^{13}C NMR spectra were obtained in $CDCl_3$ or DMSO-d_6 using a Bruker AMX400 spectrometer operating at 400.14 MHz for proton and 100.23 MHz for carbon nuclei. Chemical shifts are in parts per million and are referenced using an internal TMS standard. Mass spectra were obtained using Micromass Q-TOF-2 spectrometer for ESI.

The phospholipids 1,2-diphytanoyl-*sn*-glycerol-3-phosphocholine (DPhPC) and 1,2-dioleoyl-*sn*-glycero-3-phosphocholine (DOPC) were purchased from Avanti Polar Lipids.

Mutation K234C and Purification. Gp10-K234C plasmids were constructed from vector pET-21a(+) (Novagen) with a two-step PCR. First, primer pair F1-R1 was used to amplify gp10 gene from phi29 genome DNA-gp3, and the first PCR product was used as the template for following PCR with primer pair F2-R2 incorporating restriction sites and affinity tags. The second PCR product was digested with *Nde* I-*Xho* I and ligated into the *Nde* I-*Xho* I sites of the vector pET-21a(+).[45]

The plasmids constructed previously were transformed into the *E. coli* strain HMS174 (DE3) for protein expression. Ten milliliter overnight cell cultures were grown at 37 °C in Luria−Bertani (LB) medium containing 100 μg/mL ampicillin with shaking at 250 rpm. One percent inoculation was used for 500 mL of culture, and 0.5 mM IPTG induction was applied when OD_{600} reached 0.5−0.6. Cells were harvested 3 h post-induction by centrifugation at 5000*g* for 20 min in a Beckman JS-7.5 rotor, followed by French Press, and digested with DNase I and RNase A on ice for half an hour. Cell lysate was clarified by centrifugation and filtration.

Purification of mutant K234C-His-tagged connector proteins was conducted with one-step immobilized metal affinity chromatography (IMAC) under native conditions. Ni-NTA His-bind resin (Novagen, San Diego, CA) was packed to a column and regenerated with charge buffer (50 mM $NiCl_2$). Cell pellets were resuspended in His-bind buffer (15% glycerol, 500 mM NaCl, 10 mM imidazole, and 100 mM Tris-HCl, pH 8.0). Cell lysate was clarified by centrifugation and filtration followed by loading onto His-bind resin by gravity flow. Five column volumes (CV) of His-wash buffer (15% glycerol, 500 mM NaCl, 50 mM imidazole, and 100 mM Tris-HCl, pH 8.0) was used to remove contaminant proteins. Three to five CV of His-elute buffer (15% glycerol, 500 mM NaCl, 500 mM imidazole, and 100 mM Tris-HCl, pH 8.0) was applied to elute His-tagged gp10 protein.

Preparation of Lipid Vesicles Containing the Mutant K234C Connector Channels. The preparation of connector reconstituted liposomes has been described previously.[41] Briefly, 1 mL of 1 mg/mL DOPC in chloroform was syringed in a round-bottomed flask. The chloroform was removed under vacuum using the rotary evaporator (Buchi). The lipid film was then rehydrated with 1 mL of connector protein solution in a buffer containing 10 mM Tris/pH 7.9, 1 M NaCl, and 250 mM sucrose to bud off vesicles into the solution. The lipid solution was then extruded through a polycarbonate membrane filter (100 or 400 nm) to generate unilamellar lipid vesicles. A final molar ratio of lipid *versus* connector was established at 4000:1 to 16000:1.[41−43]

Insertion of the Connector into Planar Bilayer Lipid Membrane. The insertion of the connector reconstituted liposomes into a lipid bilayer has been described previously.[41] Briefly, a standard BLM cell was utilized to form a free-standing lipid bilayer. An aperture of 100 or 200 μm in diameter in a thin Teflon partition separated the cell into *cis*- and *trans*-compartments. After the aperture was prepainted with 0.5 μL of 3% (w/v) DPhPC *n*-decane solution twice to ensure the complete coating of the entire edge of the aperture, these compartments were filled with conducting buffers (10 mM Tris/pH 7.9, 1 M NaCl). After confirming the formation of the lipid bilayer, the connector reconstituted lipid vesicles (0.5−2 μL) was directly incubated to fuse with the planar lipid membrane.

Measurements of Current for Each Membrane Embedded Channel. A pair of Ag/AgCl electrodes connected directly to both the compartments was used to measure the current traces across the bilayer lipid membrane. The current trace was recorded using an Axopatch 200B patch clamp amplifier coupled with the Axon DigiData 1322A analog-digital converter (Axon Instruments) or the BLM workstation (Warner Instruments). All voltages reported were those of the *trans*-compartment. Data were low bandpass filtered at a frequency of 5 or 1 kHz and acquired at a sampling frequency of 20 or 200 kHz. The PClamp 9.1 software (Axon Instruments) was used to collect the data, and the software Origin Pro 8.0 was used for data analysis.

For all binding experiments, the thioesters (10 nM to 1 μM final concentration) were premixed in the conducting buffer (10 mM Tris/pH 7.9, 1 M NaCl). Upon formation of a stable bilayer, the current traces were then recorded over a period of 2−4 h.

Synthesis of Various Thioesters. The synthesis of the thioesters was accomplished using a slight modification of the route developed by Ghadiri *et al.*[78] Synthesis of the ethylthioester will be used as an example. A 0.30 g (40 mmol) sample of propanoic acid and a 0.66 g (41 mmol) sample of CDI were dissolved in 20 mL of freshly distilled $CHCl_3$. The reaction mixture was refluxed for 3 h before it was allowed to come to room temperature. Once the solution was cooled, a 0.430 g (40 mmol) sample of methylthioglycolate was added. This reaction mixture was left overnight. The solvent was removed under reduced pressure and partitioned between a 0.01 molar sodium hydroxide solution and dichloromethane. The organic layer was collected and dried over sodium sulfate. After removing the solvent under vacuum, crude material was separated *via* flash chromatography with CH_2Cl_2/hexane 80:20 (v/v) as eluent. Ethylthioester was obtained as a colorless oil (0.30 g,18 mmol) in a 46% yield.

Chemical Characterization of Various Thioesters. ^{1}H NMR ($CHCl_3$-*d*): δ 3.69 (3H, s), 3.65 (2H s), 2.58 (2H q, J = 7.6 Hz), 1.12 (3H t, J = 7.6 Hz). ^{13}C NMR ($CHCl_3$-*d*): δ 198.1, 169.3, 52.7, 37.0, 30.9, 9.4. MS: calcd mass 185.0248 for $C_6H_{10}O_3SNa^+$ [M + Na^+] found 185.0268. For thymine (14% yield) and phenyl (95% yield) thioesters, chemical analysis matched literature results. Provided also is the chemical analysis of the phenyl ester, which is not provided in the literature. ^{1}H NMR ($CHCl_3$-*d*): δ 7.91 (2H d, J = 7.6 Hz), 7.54 (1H t, J = 7.6 Hz), 7.39 (2H t, J = 7.6 Hz), 3.84 (2H, s),

3.70 (3H s). ^{13}C NMR ($CHCl_3$-*d*): δ 183.9, 172.2, 133.8, 130.1, 129.3, 128.5, 53.0, 31.4. MS: calcd mass 233.0248 for $C_{10}H_{10}O_3SNa^+$ [M + Na^+] found 233.0110.

Conflict of Interest: The authors declare the following competing financial interest(s): P.G. is a co-founder of Kylin Therapeutics, Inc., and Biomotor and Nucleic Acid Nanotechnology Development Corp. Ltd.

Acknowledgment. Research was supported by NIH Grant EB012135 (P.G.). The content is solely the responsibility of the authors and does not necessarily represent the official views of NIH NIBIB and NIGMS. The authors thank Randall Reif and Hui Zhang for assistance with data analysis.

REFERENCES AND NOTES

1. Rao, V. B.; Feiss, M. The Bacteriophage DNA Packaging Motor. *Annu. Rev. Genet.* **2008**, *42*, 647–681.
2. Guo, P. X.; Lee, T. J. Viral Nanomotors for Packaging of dsDNA and dsRNA. *Mol. Microbiol.* **2007**, *64*, 886–903.
3. Sun, S.; Rao, V. B.; Rossmann, M. G. Genome Packaging in Viruses. *Curr. Opin. Struct. Biol.* **2010**, *20*, 114–120.
4. Guo, P. Structure and Function of Phi29 Hexameric RNA That Drive Viral DNA Packaging Motor: Review. *Prog. Nucleic Acid Res. Mol. Biol.* **2002**, *72*, 415–472.
5. Aathavan, K.; Politzer, A. T.; Kaplan, A.; Moffitt, J. R.; Chemla, Y. R.; Grimes, S.; Jardine, P. J.; Anderson, D. L.; Bustamante, C. Substrate Interactions and Promiscuity in a Viral DNA Packaging Motor. *Nature* **2009**, *461*, 669–673.
6. Simpson, A. A.; Leiman, P. G.; Tao, Y.; He, Y.; Badasso, M. O.; Jardine, P. J.; Anderson, D. L.; Rossman, M. G. Structure Determination of the Head−Tail Connector of Bacteriophage Phi29. *Acta Crystallogr.* **2001**, *D57*, 1260–1269.
7. Guasch, A.; Pous, J.; Ibarra, B.; Gomis-Ruth, F. X.; Valpuesta, J. M.; Sousa, N.; Carrascosa, J. L.; Coll, M. Detailed Architecture of a DNA Translocating Machine: The High-Resolution Structure of the Bacteriophage Phi29 Connector Particle. *J. Mol. Biol.* **2002**, *315*, 663–676.
8. Zhang, F.; Lemieux, S.; Wu, X.; St.-Arnaud, S.; Mcmurray, C. T.; Major, F.; Anderson, D. Function of Hexameric RNA in Packaging of Bacteriophage Phi29 DNA *in Vitro*. *Mol. Cell* **1998**, *2*, 141–147.
9. Guo, P.; Erickson, S.; Anderson, D. A Small Viral RNA Is Required for *In Vitro* Packaging of Bacteriophage Phi29 DNA. *Science* **1987**, *236*, 690–694.
10. Guo, P.; Zhang, C.; Chen, C.; Trottier, M.; Garver, K. Inter-RNA Interaction of Phage Phi29 pRNA To Form a Hexameric Complex for Viral DNA Transportation. *Mol. Cell* **1998**, *2*, 149–155.
11. Shu, D.; Zhang, H.; Jin, J.; Guo, P. Counting of Six pRNAs of Phi29 DNA-Packaging Motor with Customized Single Molecule Dual-View System. *EMBO J.* **2007**, *26*, 527–537.
12. Sun, S.; Kondabagil, K.; Draper, B.; Alam, T. I.; Bowman, V. D.; Zhang, Z.; Hegde, S.; Fokine, A.; Rossmann, M. G.; Rao, V. B. The Structure of the Phage T4 DNA Packaging Motor Suggests a Mechanism Dependent on Electrostatic Forces. *Cell* **2008**, *135*, 1251–1262.
13. Al-Zahrani, A. S.; Kondabagil, K.; Gao, S.; Kelly, N.; Ghosh-Kumar, M.; Rao, V. B. The Small Terminase, Gp16, of Bacteriophage T4 Is a Regulator of the DNA Packaging Motor. *J. Biol. Chem.* **2009**, *284*, 24490–24500.
14. Ray, K.; Sabanayagam, C. R.; Lakowicz, J. R.; Black, L. W. DNA Crunching by a Viral Packaging Motor: Compression of a Procapsid-Portal Stalled Y-DNA Substrate. *Virology* **2010**, *398*, 224–232.
15. Sun, S. Y.; Kondabagil, K.; Gentz, P. M.; Rossmann, M. G.; Rao, V. B. The Structure of the ATPase That Powers DNA Packaging into Bacteriophage T4 Procapsids. *Mol. Cell* **2007**, *25*, 943–949.
16. Alam, T. I.; Rao, V. B. The ATPase Domain of the Large Terminase Protein, Gp17, from Bacteriophage T4 Binds DNA: Implications to the DNA Packaging Mechanism. *J. Mol. Biol.* **2008**, *376*, 1272–1281.
17. Catalano, C. E.; Cue, D.; Feiss, M. Virus DNA Packaging: The Strategy Used by Phage Lambda. *Mol. Microbiol.* **1995**, *16*, 1075–1086.
18. Hwang, Y.; Catalano, C. E.; Feiss, M. Kinetic and Mutational Dissection of the Two ATPase Activities of Terminase, the DNA Packaging Enzyme of Bacteriophage Lambda. *Biochemistry* **1996**, *35*, 2796–2803.
19. Fuller, D. N.; Raymer, D. M.; Rickgauer, J. P.; Robertson, R. M.; Catalano, C. E.; Anderson, D. L.; Grimes, S.; Smith, D. E. Measurements of Single DNA Molecule Packaging Dynamics in Bacteriophage Lambda Reveal High Forces, High Motor Processivity, and Capsid Transformations. *J. Mol. Biol.* **2007**, *373*, 1113–1122.
20. Tsay, J. M.; Sippy, J.; Feiss, M.; Smith, D. E. The Q Motif of a Viral Packaging Motor Governs Its Force Generation and Communicates ATP Recognition to DNA Interaction. *Proc. Natl. Acad. Sci. U.S.A.* **2009**, *106*, 14355–14360.
21. Gertsman, I.; Gan, L.; Guttman, M.; Lee, K.; Speir, J. A.; Duda, R. L.; Hendrix, R. W.; Komives, E. A.; Johnson, J. E. An Unexpected Twist in Viral Capsid Maturation. *Nature* **2009**, *458*, 646–650.
22. Serwer, P.; Wright, E. T.; Hakala, K.; Weintraub, S. T.; Su, M.; Jiang, W. DNA Packaging-Associated Hyper-Capsid Expansion of Bacteriophage T3. *J. Mol. Biol.* **2010**, *397*, 361–374.
23. Sun, M.; Louie, D.; Serwer, P. Single-Event Analysis of the Packaging of Bacteriophage T7 DNA Concatemers *in Vitro*. *Biophys. J.* **1999**, *77*, 1627–1637.
24. Dunn, J. J.; Studier, F. W. Complete Nucleotide Sequence of Bacteriophage T7 DNA and the Locations of T7 Genetic Elements. *J. Mol. Biol.* **1983**, *166*, 477–535.
25. Urban, M.; Joubert, N.; Hocek, M.; Alexander, R. E.; Kuchta, R. D. Herpes Simplex Virus-1 DNA Primase: A Remarkably Inaccurate Yet Selective Polymerase. *Biochemistry* **2009**, *48*, 10866–10881.
26. Newcomb, W. W.; Juhas, R. M.; Thomsen, D. R.; Homa, F. L.; Burch, A. D.; Weller, S. K.; Brown, J. C. The UL6 Gene Product Forms the Portal for Entry of DNA into the Herpes Simplex Virus Capsid. *J. Virol.* **2001**, *75*, 10923–10932.
27. Yu, D.; Weller, S. K. Generic Analysis of the UL15 Gene Locus for the Putative Terminase of Herpes Simplex Virus Type 1. *Virology* **1998**, *243*, 32–44.
28. Salmon, B.; Baines, J. D. Herpes Simplex Virus DNA Cleavage and Packaging: Association of Multiple Forms of U(L)15-Encoded Proteins with B Capsids Requires at Least the U(L)6, U(L)17, and U(L)28 Genes. *J. Virol.* **1998**, *72*, 3045–3050.
29. Roos, W. H.; Radtke, K.; Kniesmeijer, E.; Geertsema, H.; Sodeik, B.; Wuite, G. J. Scaffold Expulsion and Genome Packaging Trigger Stabilization of Herpes Simplex Virus Capsids. *Proc. Natl. Acad. Sci. U.S.A.* **2009**, *106*, 9673–9678.
30. Schmid, S. I.; Hearing, P. Bipartite Structure and Functional Independence of Adenovirus Type 5 Packaging Elements. *J. Virol.* **1997**, *71*, 3375–3384.
31. Bett, A.; Prevec, L.; Graham, F. Packaging Capacity and Stability of Human Adenovirus Type 5 Vectors. *J. Virol.* **1993**, *67*, 5911–5921.
32. Zhang, W.; Low, J. A.; Christensen, J. B.; Imperiale, M. J. Role for the Adenovirus Iva2 Protein in Packaging of Viral DNA. *J. Virol.* **2001**, *75*, 10446–10454.
33. Koonin, E. V.; Senkevich, T. G.; Chernos, V. I. Gene-A32 Product of Vaccinia Virus May Be an ATPase Involved in Viral-DNA Packaging as Indicated by Sequence Comparisons with Other Putative Viral ATPases. *Virus Genes* **1993**, *7*, 89–94.
34. Cassetti, M. C.; Merchlinsky, M.; Wolffe, E. J.; Weiserg, A. S.; Moss, B. DNA Package Mutant: Repression of the Vaccinia Virus A32 Gene Results in Noninfectious, DNA-Deficient, Spherical, Enveloped Particles. *J. Virol.* **1998**, *72*, 5769–5780.
35. Simpson, A. A.; Tao, Y.; Leiman, P. G.; Badasso, M. O.; He, Y.; Jardine, P. J.; Olson, N. H.; Morais, M. C.; Grimes, S.; Anderson, D. L.; Baker, T. S.; Rossmann, M. G. Structure of

the Bacteriophage Phi29 DNA Packaging Motor. *Nature* **2000**, *408*, 745–750.
36. Valpuesta, J. M.; Fujisawa, H.; Marco, S.; Carazo, J. M.; Carrascosa, J. Three-Dimensional Structure of T3 Connector Purified from Overexpressing Bacteria. *J. Mol. Biol.* **1992**, *224*, 103–112.
37. Rishovd, S.; Holzenburg, A.; Johansen, B. V.; Lindqvist, B. H. Bacteriophage P2 and P4 Morphogenesis: Structure and Function of the Connector. *Virology* **1998**, *245*, 11–17.
38. Kochan, J.; Carrascosa, J. L.; Murialdo, H. Bacteriophage Lambda Preconnectors: Purification and Structure. *J. Mol. Biol.* **1984**, *174*, 433–447.
39. Donate, L. E.; Herranz, L.; Secilla, J. P.; Carazo, J. M.; Fujisawa, H.; Carrascosa, J. L. Bacteriophage T3 Connector: Three-Dimensional Structure and Comparison with Other Viral Head–Tail Connecting Regions. *J. Mol. Biol.* **1988**, *201*, 91–100.
40. Bazinet, C.; King, J. The DNA Translocation Vertex of dsDNA Bacteriophages. *Annu. Rev. Microbiol.* **1985**, *39*, 109–129.
41. Wendell, D.; Jing, P.; Geng, J.; Subramaniam, V.; Lee, T. J.; Montemagno, C.; Guo, P. Translocation of Double-Stranded DNA through Membrane-Adapted Phi29 Motor Protein Nanopores. *Nat. Nanotechnol.* **2009**, *4*, 765–772.
42. Jing, P.; Haque, F.; Vonderheide, A.; Montemagno, C.; Guo, P. Robust Properties of Membrane-Embedded Connector Channel of Bacterial Virus Phi29 DNA Packaging Motor. *Mol. Biosyst.* **2010**, *6*, 1844–1852.
43. Jing, P.; Haque, F.; Shu, D.; Montemagno, C.; Guo, P. One-Way Traffic of a Viral Motor Channel for Double-Stranded DNA Translocation. *Nano Lett.* **2010**, *10*, 3620–3627.
44. Cai, Y.; Xiao, F.; Guo, P. The Effect of N- or C-Terminal Alterations of the Connector of Bacteriophage Phi29 DNA Packaging Motor on Procapsid Assembly, pRNA Binding, and DNA Packaging. *Nanomedicine* **2008**, *4*, 8–18.
45. Robinson, M. A.; Wood, J. P.; Capaldi, S. A.; Baron, A. J.; Gell, C.; Smith, D. A.; Stonehouse, N. J. Affinity of Molecular Interactions in the Bacteriophage Phi29 DNA Packaging Motor. *Nucleic Acids Res.* **2006**, *34*, 2698–2709.
46. Sun, J.; Cai, Y.; Moll, W. D.; Guo, P. Controlling Bacteriophage Phi29 DNA-Packaging Motor by Addition or Discharge of a Peptide at N-Terminus of Connector Protein That Interacts with pRNA. *Nucleic Acids Res.* **2006**, *34*, 5482–5490.
47. Valle, M.; Kremer, L.; Martinez, A.; Roncal, F.; Valpuesta, J. M.; Albar, J. P.; Carrascosa, J. L. Domain Architecture of the Bacteriophage Phi29 Connector Protein. *J. Mol. Biol.* **1999**, *288*, 899–909.
48. Xiao, F.; Sun, J.; Coban, O.; Schoen, P.; Wang, J. C.; Cheng, R. H.; Guo, P. Fabrication Of Massive Sheets of Single Layer Patterned Arrays Using Reengineered Phi29 Motor Dodecamer. *ACS Nano* **2009**, *3*, 100–107.
49. Xiao, F.; Cai, Y.; Wang, J. C.; Green, D.; Cheng, R. H.; Demeler, B.; Guo, P. Adjustable Ellipsoid Nanoparticles Assembled from Re-engineered Connectors of the Bacteriophage Phi29 DNA Packaging Motor. *ACS Nano* **2009**, *3*, 2163–2170.
50. Xiao, F.; Demeler, B.; Guo, P. Assembly Mechanism of the Sixty-Subunit Nanoparticles *via* Interaction of RNA with the Reengineered Protein Connector of Phi29 DNA-Packaging Motor. *ACS Nano* **2010**, *4*, 3293–3301.
51. Ibanez, C.; Garcia, J. A.; Carrascosa, J. L.; Salas, M. Overproduction and Purification of the Connector Protein of *Bacillus subtilis* Phage Φ29. *Nucleic Acids Res.* **1984**, *12*, 2351–2365.
52. Guo, Y.; Blocker, F.; Xiao, F.; Guo, P. Construction and 3-D Computer Modeling of Connector Arrays with Tetragonal to Decagonal Transition Induced By pRNA of Phi29 DNA-Packaging Motor. *J. Nanosci. Nanotechnol.* **2005**, *5*, 856–863.
53. Braha, O.; Gu, L. Q.; Zhou, L.; Lu, X.; Cheley, S.; Bayley, H. Simultaneous Stochastic Sensing of Divalent Metal Ions. *Nat. Biotechnol.* **2000**, *18*, 1005–1007.
54. Nakane, J.; Wiggin, M.; Marziali, A. A Nanosensor for Transmembrane Capture and Identification of Single Nucleic Acid Molecules. *Biophys. J.* **2004**, *87*, 615–621.
55. Gao, C.; Ding, S.; Tan, Q.; Gu, L. Q. Method of Creating a Nanopore-Terminated Probe for Single-Molecule Enantiomer Discrimination. *Anal. Chem.* **2009**, *81*, 80–86.
56. Wang, J.; Martin, C. R. A New Drug-Sensing Paradigm Based on Ion-Current Rectification in a Conically Shaped Nanopore. *Nanomedicine* **2008**, *3*, 13–20.
57. Rodrigues, C. G.; Machado, D. C.; Chevtchenko, S. F.; Krasilnikov, O. V. Mechanism of KCl Enhancement in Detection of Nonionic Polymers by Nanopore Sensors. *Biophys. J.* **2008**, *95*, 5186–5192.
58. Kasianowicz, J. J.; Brandin, E.; Branton, D.; Deamer, D. W. Characterization of Individual Polynucleotide Molecules Using a Membrane Channel. *Proc. Natl. Acad. Sci. U.S.A.* **1996**, *93*, 13770–13773.
59. Benner, S.; Chen, R. J. A.; Wilson, N. A.; Bu-Shumays, R.; Hurt, N.; Lieberman, K. R.; Deamer, D. W.; Dunbar, W. B.; Akeson, M. Sequence-Specific Detection of Individual DNA Polymerase Complexes in Real Time Using a Nanopore. *Nat. Nanotechnol.* **2007**, *2*, 718–724.
60. Stoddart, D.; Heron, A. J.; Mikhailova, E.; Maglia, G.; Bayley, H. Single-Nucleotide Discrimination in Immobilized DNA Oligonucleotides with a Biological Nanopore. *Proc. Natl. Acad. Sci. U.S.A.* **2009**, *106*, 7702–7707.
61. Ward, P. L.; Roizman, B. Herpes Simplex Genes: The Blueprint of a Successful Human Pathogen [Published Erratum Appears in *Trends Genet.* **1994** Oct;10(10):380]. *Trends Genet.* **1994**, *10*, 267–274.
62. Meller, A.; Nivon, L.; Brandin, E.; Golovchenko, J.; Branton, D. Rapid Nanopore Discrimination between Single Polynucleotide Molecules. *Proc. Natl. Acad. Sci. U.S.A.* **2000**, *97*, 1079–1084.
63. Meller, A.; Branton, D. Single Molecule Measurements of DNA Transport through a Nanopore. *Electrophoresis* **2002**, *23*, 2583–2591.
64. Meller, A. Dynamics of Polynucleotide Transport through Nanometre-Scale Pores. *J. Phys.: Condens. Matter* **2003**, *15*, R581–R607.
65. Mcnally, B.; Wanunu, M.; Meller, A. Electro-Mechanical Unzipping of Individual DNA Molecules Using Synthetic Sub-2-nm Pores. *Nano Lett.* **2008**, *8*, 3418–3422.
66. Wanunu, M.; Morrison, W.; Rabin, Y.; Grosberg, A. Y.; Meller, A. Electrostatic Focusing of Unlabelled DNA into Nanoscale Pores Using a Salt Gradient. *Nat. Nanotechnol.* **2010**, *5*, 160–165.
67. Vercoutere, W.; Winters-Hilt, S.; Olsen, H.; Deamer, D.; Haussler, D.; Akeson, M. Rapid Discrimination among Individual DNA Hairpin Molecules at Single-Nucleotide Resolution Using an Ion Channel. *Nat. Biotechnol.* **2001**, *19*, 248–252.
68. Vercoutere, W. A.; Winters-Hilt, S.; Deguzman, V. S.; Deamer, D.; Ridino, S. E.; Rodgers, J. T.; Olsen, H. E.; Marziali, A.; Akeson, M. Discrimination among Individual Watson–Crick Base Pairs at the Termini of Single DNA Hairpin Molecules. *Nucleic Acids Res.* **2003**, *31*, 1311–1318.
69. Iqbal, S. M.; Akin, D.; Bashir, R. Solid-State Nanopore Channels with DNA Selectivity. *Nat. Nanotechnol.* **2007**, *2*, 243–248.
70. Venkatesan, M.; Yemenicioglu, S.; Dorvel, B.; Bashir, R. Fabrication and Characterization of Low Stress, Mechanically Robust Al_2O_3 Nanopores for the Electronic Detection of Biomolecules. *Adv. Mater.* **2009**, *21*, 1–6.
71. Bayley, H.; Cremer, P. S. Stochastic Sensors Inspired by Biology. *Nature* **2001**, *413*, 226–230.
72. Raj, A.; Van, O. A. Single-Molecule Approaches to Stochastic Gene Expression. *Annu. Rev. Biophys.* **2009**, *38*, 255–270.
73. Perkins, T. J.; Swain, P. S. Strategies for Cellular Decision-Making. *Mol. Syst. Biol.* **2009**, *5*, 326.
74. Thomson, K.; Amin, I.; Morales, E.; Winters-Hilt, S. Preliminary Nanopore Cheminformatics Analysis of Aptamer-Target Binding Strength. *BMC Bioinf.* **2007**, *8*, S11.

75. Winters-Hilt, S. Nanopore Detector Based Analysis of Single-Molecule Conformational Kinetics and Binding Interactions. *BMC Bioinf.* **2006**, *7*, S21.
76. Bayley, H.; Martin, C. R. Resistive-Pulse Sensing: From Microbes to Molecules. *Chem. Rev.* **2000**, *100*, 2575–2594.
77. Sauer-Budge, A. F.; Nyamwanda, J. A.; Lubensky, D. K.; Branton, D. Unzipping Kinetics of Double-Stranded DNA in a Nanopore. *Phys. Rev. Lett.* **2003**, *90*, 238101.
78. Ura, Y.; Beierle, J. M.; Leman, L. J.; Orgel, L. E.; Ghadiri, M. R. Self-Assembling Sequence-Adaptive Peptide Nucleic Acids. *Science* **2009**, *325*, 73–77.
79. Carazo, J.; Santisteban, A.; Carrascosa, J. Three-Dimensional Reconstruction of Bacteriophage Φ29 Neck Particles at 2.2 nm Resolution. *J. Mol. Biol.* **1985**, *183*, 79–88.
80. Jimenez, J.; Santisteban, A.; Carazo, J. M.; Carrascosa, J. L. Computer Graphic Display Method for Visualizing Three-Dimensional Biological Structures. *Science* **1986**, *232*, 1113–1115.
81. Carazo, J. M.; Donate, L. E.; Herranz, L.; Secilla, J. P.; Carrascosa, J. L. Three-Dimensional Reconstruction of the Connector of Bacteriophage Φ29 at 1.8 nm Resolution. *J. Mol. Biol.* **1986**, *192*, 853–867.
82. Endo, T.; Kerman, K.; Nagatani, N.; Hiepa, H. M.; Kim, D. K.; Yonezawa, Y.; Nakano, K.; Tamiya, E. Multiple Label-Free Detection of Antigen−Antibody Reaction Using Localized Surface Plasmon Resonance-Based Core−Shell Structured Nanoparticle Layer Nanochip. *Anal. Chem.* **2006**, *78*, 6465–6475.
83. Hirsch, L. R.; Jackson, J. B.; Lee, A.; Halas, N. J.; West, J. L. A Whole Blood Immunoassay Using Gold Nanoshells. *Anal. Chem.* **2003**, *75*, 2377–2381.
84. Cao, Y. C.; Jin, R.; Nam, J. M.; Thaxton, C. S.; Mirkin, C. A. Raman Dye-Labeled Nanoparticle Probes for Proteins. *J. Am. Chem. Soc.* **2003**, *125*, 14676–14677.
85. Roll, D.; Malicka, J.; Gryczynski, I.; Gryczynski, Z.; Lakowicz, J. R. Metallic Colloid Wavelength-Ratiometric Scattering Sensors. *Anal. Chem.* **2003**, *75*, 3440–3445.
86. Haes, A. J.; Van Duyne, R. P. A Nanoscale Optical Biosensor: Sensitivity and Selectivity of an Approach Based on the Localized Surface Plasmon Resonance Spectroscopy of Triangular Silver Nanoparticles. *J. Am. Chem. Soc.* **2002**, *124*, 10596–10604.
87. Riboh, J. C.; Haes, A. J.; Mcfarland, A. D.; Yonzon, C. R.; Van Duyne, R. P. A Nanoscale Optical Biosensor: Real-Time Immunoassay in Physiological Buffer Enabled by Improved Nanoparticle Adhesion. *J. Phys. Chem. B* **2003**, *107*, 1772–1780.
88. Marinakos, S. M.; Chen, S.; Chilkoti, A. Plasmonic Detection of a Model Analyte in Serum by a Gold Nanorod Sensor. *Anal. Chem.* **2007**, *79*, 5278–5283.
89. Guo, Y.; Ye, J. Y.; Divin, C.; Huang, B.; Thomas, T. P.; Baker, J. R., Jr.; Norris, T. B. Real-Time Biomolecular Binding Detection Using a Sensitive Photonic Crystal Biosensor. *Anal. Chem.* **2010**, *82*, 5211–5218.
90. Niemeyer, C. M.; Ceyhan, B. DNA-Directed Functionalization of Colloidal Gold with Proteins. *Angew. Chem., Int. Ed.* **2001**, *40*, 3685–3688.
91. Mor, G.; Visintin, I.; Lai, Y.; Zhao, H.; Schwartz, P.; Rutherford, T.; Yue, L.; Bray-Ward, P.; Ward, D. C. Serum Protein Markers for Early Detection of Ovarian Cancer. *Proc. Natl. Acad. Sci. U.S.A.* **2005**, *102*, 7677–7682.
92. Eisenstein, M. Protein Arrays: Growing Pains. *Nature* **2006**, *444*, 959–962.
93. Nettikadan, S.; Radke, K.; Johnson, J.; Xu, J.; Lynch, M.; Mosher, C.; Henderson, E. Detection and Quantification of Protein Biomarkers from Fewer than 10 Cells. *Mol. Cell Proteomics* **2006**, *5*, 895–901.
94. Yu, X.; Xu, D.; Cheng, Q. Label-Free Detection Methods for Protein Microarrays. *Proteomics* **2006**, *6*, 5493–5503.
95. Yao, Z.; Li, C.; Shi, G. Optically Active Supramolecular Complexes of Water-Soluble Achiral Polythiophenes and Folic Acid: Spectroscopic Studies and Sensing Applications. *Langmuir* **2008**, *24*, 12829–12835.
96. Ashok, P. C.; Singh, G. P.; Tan, K. M.; Dholakia, K. Fiber Probe Based Microfluidic Raman Spectroscopy. *Opt. Express* **2010**, *18*, 7642–7649.
97. Kafi, A. K.; Ahmadalinezhad, A.; Wang, J.; Thomas, D. F.; Chen, A. Direct Growth of Nanoporous Au and Its Application in Electrochemical Biosensing. *Biosens. Bioelectron.* **2010**, *25*, 2458–2463.
98. Alvarez-Puebla, R. A.; Liz-Marzan, L. M. SERS-Based Diagnosis and Biodetection. *Small* **2010**, *6*, 604–610.
99. Notingher, I. Raman Spectroscopy Cell-Based Biosensors. *Sensors* **2007**, *7*, 1343–1358.
100. Mazzitelli, C. L.; Brodbelt, J. S. Probing Ligand Binding to Duplex DNA Using Kmno4 Reactions and Electrospray Ionization Tandem Mass Spectrometry. *Anal. Chem.* **2007**, *79*, 4636–4647.
101. Ding, F. X.; Lee, B. K.; Hauser, M.; Davenport, L.; Becker, J. M.; Naider, F. Probing the Binding Domain of the *Saccharomyces cerevisiae* Alpha-Mating Factor Receptor with Fluorescent Ligands. *Biochemistry* **2001**, *40*, 1102–1108.
102. Shanmukh, S.; Jones, L.; Driskell, J.; Zhao, Y.; Dluhy, R.; Tripp, R. A. Rapid and Sensitive Detection of Respiratory Virus Molecular Signatures Using a Silver Nanorod Array SERS Substrate. *Nano Lett.* **2006**, *6*, 2630–2636.
103. Liu, F.; Dubey, M.; Takahashi, H.; Castner, D. G.; Grainger, D. W. Immobilized Antibody Orientation Analysis Using Secondary Ion Mass Spectrometry and Fluorescence Imaging of Affinity-Generated Patterns. *Anal. Chem.* **2010**, *82*, 2947–2958.
104. Nath, N.; Chilkoti, A. A Colorimetric Gold Nanoparticle Sensor To Interrogate Biomolecular Interactions in Real Time on a Surface. *Anal. Chem.* **2002**, *74*, 504–509.
105. Geng, J.; Fang, H.; Haque, F.; Zhang, L.; Guo, P. Three Reversible and Controllable Discrete Steps of Channel Gating of a Viral DNA Packaging Motor. *Biomaterials* **2011**, *32*, 8234–8242.
106. Fang, H.; Jing, P.; Haque, F.; Guo, P. Role of Channel Lysines and The "Push Through a One-way Valve" Mechanism of the Viral DNA Packaging Motor. *Biophys. J.* **2012**, *102*, 127–135.